PHYSICAL REVIEW E **90**, 041002(R) (2014)

Bathtub vortex induced by instability

Jiro Mizushima and Kazuki Abe
Department of Mechanical Engineering, Doshisha University, Kyotanabe, Kyoto 610-0321, Japan

Naoto Yokoyama
Department of Aeronautics and Astronautics, Kyoto University, Kyoto, Kyoto 615-8540, Japan

(Received 26 May 2014; published 17 October 2014)

The driving mechanism and the swirl direction of the bathtub vortex are investigated by the linear stability analysis of the no-vortex flow as well as numerical simulations. We find that only systems having plane symmetries with respect to vertical planes deserve research for the swirl direction. The bathtub vortex appearing in a vessel with a rectangular cross section having a drain hole at the center of the bottom is proved to be induced by instability when the flow rate exceeds a threshold. The Coriolis force is capable of determining the swirl direction to be cyclonic.

DOI: 10.1103/PhysRevE.90.041002 PACS number(s): 47.15.Fe, 47.20.Ky, 47.32.C−, 47.32.Ef

Vortical flows are often observed in bathtubs or washbowls in our daily life, and have attracted the intense interest of not only physicists but also persons on the street. Despite wide and intense interest, few reports have been published on the bathtub vortex, and the conclusions drawn are not so definite as to convince us of the generation mechanism. This difficulty comes from the ambiguity in the problem definition, i.e., the lack of symmetry consideration.

Shapiro [1] may be the first who carried out systematic and careful experiments to resolve this problem. He performed the experiments in Boston with a cylindrical tank. He found that the swirl direction of the vortex was mostly counterclockwise. Then, he concluded that the bathtub vortex is produced by the Coriolis force, which was supported by the experiments made in Sydney in the southern hemisphere [2]. The conclusion that no angular momentum can be supplied by viscous stress or pressure in the axisymmetric systems is consistent with Noether's theorem. Note that the axisymmetric system represents that both flow and vessel have axisymmetry.

Recently Shapiro's conclusion was numerically confirmed based on the assumption of axisymmetry [3]. It showed that the formation of a bathtub vortex is a transient phenomenon resulting from accumulation of the residual vorticity, and the vortex decays eventually if the bathtub is set on a stationary base. When the whole system rotates like on the earth, another steady bathtub vortex appears owing to the Coriolis force after decay of the transient vortex. Thus, it was confirmed that the Coriolis force is the sole origin of the steady bathtub vortex in the axisymmetric system.

In a vessel without any symmetry, the flow induced owing to drainage has a finite angular momentum in total with respect to the center of the drain hole, and hence a vortex appears above the drain hole as a result of accumulation of angular momentum conveyed by gathering fluid. For example, if the drain hole is neither on the two symmetric planes in a rectangular vessel, then fluid particles, possessing their own local angular momentum, come toward the drain hole accompanying their angular momentum to yield a bathtub vortex as a result of accumulation of the local angular momentum.

Therefore, only systems without axisymmetry but having plane symmetries deserve research for the generation mechanism of the bathtub vortex. Earlier experimental studies for the systems with one or two plane symmetries often adopt a rectangular vessel as in Refs. [4–6], where it was concluded that formation of the vortex is a phase transition, and the threshold of the discharge rate was determined. We will confirm that the bathtub vortex is induced by instability of the no-vortex flow in the systems having two plane symmetries and clarify the driving mechanism of the vortex in this Rapid Communication.

We consider the water flow in a rectangular tank with a square drain hole at the center of the bottom, to which a drain pipe is connected (Fig. 1). The side length of the drain hole is defined as d, and the drain pipe length is $\ell = 5d$. The dimensions of the tank are $a = 10d$ in length and $b = 3d$ in width. We take the coordinates as shown in Fig. 1. Water is always filled up to the height of $h = d$ by a continuous supply through the two inlets at the top of the two facing sidewalls at $x = \pm a/2 = \pm 5d$, and the water surface is assumed to be flat even after a bathtub vortex appeared. The correction due to the effects of surface deformation and surface tension was discussed in Ref. [7].

The time evolution of the incompressible flow is governed by the continuity and the Navier-Stokes (NS) equation for the velocity $\boldsymbol{u} = (u, v, w)$ and the pressure p, which are expressed in nondimensional form as

$$\nabla \cdot \boldsymbol{u} = 0, \quad \frac{\partial \boldsymbol{u}}{\partial t} + (\boldsymbol{u} \cdot \nabla)\boldsymbol{u} + \frac{1}{\mathrm{Ro}} \boldsymbol{e}_z \times \boldsymbol{u} = -\nabla p + \frac{1}{\mathrm{Re}} \Delta \boldsymbol{u}, \tag{1}$$

where we have chosen the side length d of the drain hole and the mean velocity $\bar{w} = Q/d^2$ at the outlet as the characteristic length and velocity scales, Q being the flow rate of water through the drain pipe. The nondimensional parameters are the Reynolds number $\mathrm{Re} = Q/(\nu d)$ and the Rossby number $\mathrm{Ro} = Q/(2\Omega d^3)$, where ν is the kinematic viscosity of water and Ω the angular velocity of the system about the z axis. No gravitational force term appears in the NS equation, because the effect of the gravity is incorporated into the pressure term.

The boundary conditions for the flow are stress-free at the flat water surface, and non slip on the solid walls and the bottom. The velocities of incoming flow through the inlets, $AA'D'D$ and $EE'H'H$ ($x = \pm 5$, $-3/2 \leqslant y \leqslant 3/2$, $3/4 \leqslant$

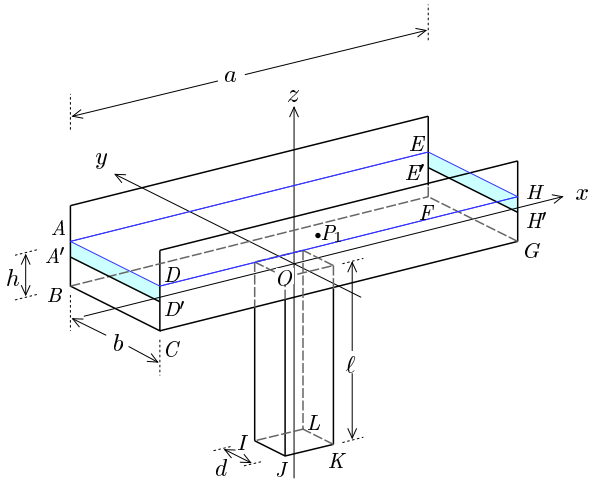

FIG. 1. (Color online) Computational model and coordinates.

$z \leqslant 1$), are assumed to have parabolic profiles in the y direction and to be uniform in the z direction as $u = \mp[1 - (2y/3)^2]$. The total inflow of the z component of angular momentum coming through the two inlets vanishes because of the plane symmetry of the inflow velocity profile. At the outlet, $IJKL$, the natural outflow condition is used. The pressure is set as $p = 0$ at the center of the outlet. On the other boundaries the pressure gradients are evaluated from the NS equation and used as the boundary conditions in solving the Poisson equation for the pressure.

We choose the y component of velocity v_1 at the point P_1 $[(x,y,z) = (1/2,0,1/2)]$, above the edge of the drain hole, as the representative physical quantity to characterize the flow field. The total angular momentum in the z direction M_z in the whole flow field is also employed to characterize the appearance of the vortex.

We use two different methods to explore the origin of the bathtub vortex. One is simulations to solve Eq. (1) numerically as an initial-value boundary-value problem by the marker-and-cell (MAC) method, and the other is a linear stability analysis of the no-vortex flow. The second-order central-difference scheme with the staggered grid with a grid spacing 0.05 is used for evaluation of the derivatives in all the numerical calculations. The Euler method with time step 5×10^{-3} is employed for the time integration of the NS equation for the velocity. The successive overrelaxation (SOR) method is employed to solve the Poisson equation for the pressure. The numerical accuracy is evaluated in the Supplemental Material [8].

The flow becomes steady having no vortex after long time elapsed independently of the initial condition if Re is smaller than a critical value. To investigate the instability of the no-vortex flow, $(\overline{\boldsymbol{u}}, \overline{p})$, we express $\boldsymbol{u} = \overline{\boldsymbol{u}} + \widehat{\boldsymbol{u}}$ and $p = \overline{p} + \widehat{p}$, where $(\widehat{\boldsymbol{u}}, \widehat{p})$ is a disturbance. From Eq. (1), we obtain the linearized disturbance equations for $(\widehat{\boldsymbol{u}}, \widehat{p})$, which are solved numerically in the same way as Eq. (1).

We have performed numerical simulation of the flow for $50 \leqslant \mathrm{Re} \leqslant 200$, adopting the no-vortex flow for the initial condition, which is obtained in advance under the symmetry conditions with respect to the yz and xz planes at $\mathrm{Re} = 50$. In this Rapid Communication, the rotation-free system, i.e., $\mathrm{Ro} = \infty$ is mostly considered, while the effect of the Coriolis force is discussed in the bifurcation structure (Fig. 3 below), where $\mathrm{Ro} = 2.4 \times 10^5$ is used to imitate the experiment in Ref. [4].

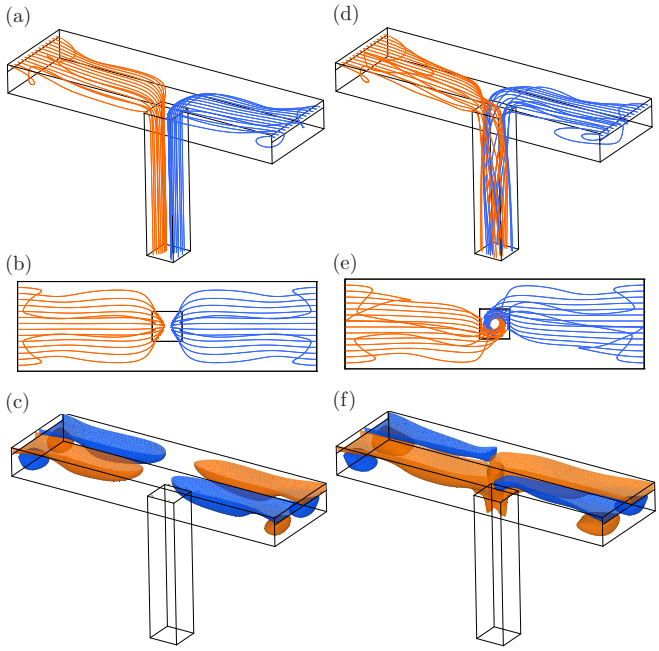

FIG. 2. (Color) Flow fields for $\mathrm{Re} = 50$ [(a)–(c)] and for $\mathrm{Re} = 100$ [(d)–(f)], where $\mathrm{Ro} = \infty$. (a), (d) Paths of fluid particles initially aligned on lines at midheight of the inlets. (b), (e) Horizontal projection of paths. (c), (f) Isosurfaces of $m_z = 0.12$ (counterclockwise, brown) and $m_z = -0.12$ (clockwise, blue).

In the numerical simulations, we found two qualitatively distinct flows. One is no-vortex and has the double-plane symmetry with respect to the yz and xz planes. The other includes the bathtub vortex having a line symmetry with respect to the z axis, being invariant under rotation by π around the z axis. In the former, fluid particles flowing in through the inlets come to gather around the central region of the tank and go down into the drain hole if Re is below a critical value. An example of the double-plane symmetric flow is shown in Figs. 2(a)–2(c) for $\mathrm{Re} = 50$. Figure 2(a) is a perspective view of paths of fluid particles initially aligned on lines at midheight of the inlets ($x = \pm 5, z = 7/8$). The fluid particles come together directly to the center of the tank without any swirling motion. The double-plane symmetry with respect to the yz and xz planes is evident in Fig. 2(b), which shows the paths projected onto a two-dimensional horizontal plane. The double-plane symmetry is equivalent to the line symmetry with respect to the z axis, i.e., invariance under rotation by π around the z axis plus the plane symmetry with respect to one of the yz and xz planes. We define the z component of the angular momentum density per unit volume as $m_z = xv - yu$, where the counterclockwise direction viewing from above is taken as positive. The isosurfaces of $m_z = \pm 0.12$ drawn in Fig. 2(c) terminate before reaching the drain hole.

The flow pattern at $\mathrm{Re} = 100$ [Figs. 2(d)–2(f)] is quite different from that observed at $\mathrm{Re} = 50$. The fluid particles coming through the inlets turn to one side before coming to the

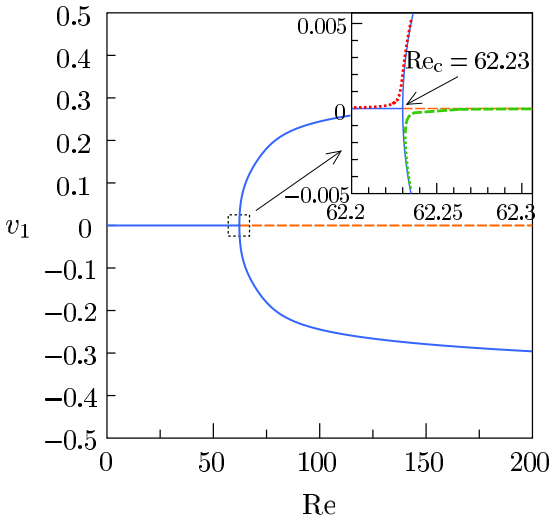

FIG. 3. (Color online) Bifurcation diagram for $\mathrm{Ro} = \infty$. $v_1 = v(\mathrm{P_1})$: Circumferential velocity at the representative point. Solid lines: Stable solutions; dashed line: unstable solution. Inset: Enlarged view of bifurcation diagram for both $\mathrm{Ro} = \infty$ (solid and dashed lines) and $\mathrm{Ro} = 2.4 \times 10^5$ (dotted lines).

center, and they are drawn into the drain pipe. The projection in Fig. 2(e) shows that the fluid particles coming from both sides meet around the z axis to be mixed up, and go through the drain pipe drawing helical paths. The isosurfaces of $m_z = 0.12$ extend from the inlets to the z axis and bend downward to the drain pipe, while those of $m_z = -0.12$ terminate before reaching the drain hole as seen in Fig. 2(f). It shows that the flow has a bathtub vortex swirling in the counterclockwise direction and that the positive angular momentum is drawn into the drain hole.

We numerically evaluated the circumferential velocity $v_1 = v(P_1)$ $[P_1 = (1/2,0,1/2)]$ in the steady state for various Re. The velocity is plotted as a function of Re in Fig. 3. In this figure, v_1 vanishes if Re is less than a critical value, which is $\mathrm{Re_c} = 62.23$. The velocity deviates from 0 above the critical value. We confirmed two different flows with positive and negative values of v_1, where the established bathtub vortex has the counterclockwise ($v_1 > 0$) or clockwise ($v_1 < 0$) direction. Furthermore, the no-vortex double-plane symmetric flow is also confirmed to be a solution of Eq. (1).

The relation $v_1^2 \propto (\mathrm{Re} - \mathrm{Re_c})$ above $\mathrm{Re_c}$ and the diagram depicted in Fig. 3 show that the appearance of the bathtub vortex is due to a pitchfork bifurcation, a symmetry-breaking bifurcation from a steady state having symmetries into another steady state having fewer symmetries. In the present case, the system had the line symmetry with respect to the z axis plus the plane symmetry with respect to one of the yz and xz planes, which is equivalent to the double-plane (the yz and xz planes) symmetry before the bifurcation. Owing to the symmetry-breaking bifurcation the system loses one plane symmetry but keeps the line symmetry. From this point of view, the line symmetry plus the plane symmetry is more natural to specify the symmetry that the system has than the double-plane symmetry, though both are equivalent. The pitchfork bifurcation caused by instability due to a stationary disturbance yields two branches, $v_1 > 0$ and $v_1 < 0$, stemming

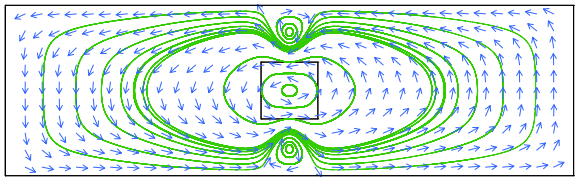

FIG. 4. (Color online) Eigenfunction of disturbance from the linear stability analysis (horizontal velocities on $z = 1/2$ and paths of fluid particles). $\mathrm{Re} = 65$; $\mathrm{Ro} = \infty$. Top view.

from that of $v_1 = 0$ at $\mathrm{Re_c}$. Either flow with positive or negative circulation emerges depending on the initial condition, and the swirl direction is not determined *a priori* unless the initial condition including the residual angular momentum is given precisely.

When Ro is finite, the system does not have the plane symmetries but has the line symmetry. Then, the bifurcation diagram is altered dramatically to be imperfect and determines the swirl direction to be cyclonic if the residual angular momentum is much smaller than the effect of the Coriolis force (inset of Fig. 3).

The linear stability analysis gives the eigenfunction of the disturbance leading to the bathtub vortex flow, which is depicted in Fig. 4. The flow field shows a global circulation in the counterclockwise direction around the z axis. Two small vortices adjacent to the long walls are important in discussion of the instability mechanism to lead the flow to self-excitation. Apparently, the counterpart obtained by reversing the circulation direction of the vortex is also a solution of the linear eigenvalue problem. This also confirms that the direction of swirl in the bathtub vortex is not uniquely determined if any initial condition is not precisely prescribed when $\mathrm{Ro} = \infty$.

We proceed to explore the physical mechanism to induce and maintain the vortical flow. Since the no-vortex flow is taken as the initial condition in all the numerical simulations, the vertical component of the total angular momentum M_z is 0 initially, but increases exponentially during a time period $t \lessapprox 300$ to attain a constant owing to the nonlinearity as seen in Fig. 5(a). The positive M_z means that the counterclockwise

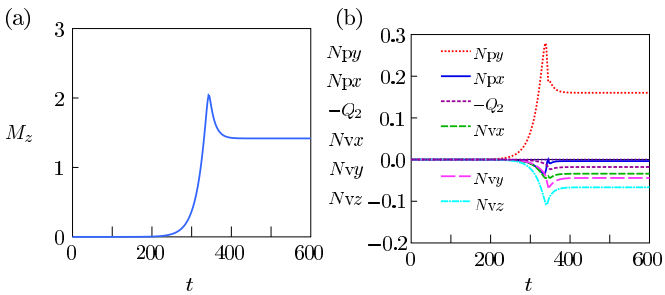

FIG. 5. (Color online) Time evolution of the total angular momentum M_z, angular momentum outflow Q_2, and torques due to pressure and viscous stress on the sidewalls and the bottom. $\mathrm{Re} = 100$; $\mathrm{Ro} = \infty$. (a) Angular momentum M_z. (b) Inflow of the angular momentum ($-Q_2$) from the outlet (Q_2: outflow); torques due to viscous stress N_{vx}, N_{vy}, and N_{vz}; torques due to pressure N_{px} and N_{py}.

rotation was chosen by chance in the present case. The time evolution of M_z is determined by the angular momentum outflow through the outlet Q_2, and torques N_{px}, N_{py}, N_{vx}, N_{vy}, and N_{vz}, where the first suffix p or v indicates that the torques come from pressure or viscous stress, respectively, and the second suffix x, y, or z shows the normal axis of the solid boundaries from which the torques are exerted on the fluid. Note that the angular momentum inflow through the inlets Q_1 always vanishes by the inflow boundary condition, and that $N_{pz} = 0$ both on the free surface and on the bottom. The torque N_{py} is exerted by the pressure on the sidewalls normal to the y axis, which is expressed as $N_{py} = -\iint_{S_{y+}} xp(x,3/2,z)dxdz + \iint_{S_{y-}} xp(x,-3/2,z)dxdz$, where $S_{y\pm}$ indicates the areas of the sidewalls at $y = \pm 3/2$. Similarly, the torque due to the viscous stress on the bottom is defined as $N_{vz} = \mathrm{Re}^{-1}\iint_{S_z}(-x\partial v/\partial z|_{z=0} + y\partial u/\partial z|_{z=0})dxdy$, where S_z denotes the area of the bottom except the drain hole. The angular momentum conservation is written as $dM_z/dt = -Q_2 + N_{px} + N_{py} + N_{vx} + N_{vy} + N_{vz}$.

The outflow Q_2 is positive having the same sign with the induced angular momentum M_z, and hence the contribution $(-Q_2)$ to the growth of M_z is negative as shown in Fig. 5(b). All the torques due to the viscous stress N_{vx}, N_{vy}, and N_{vz} are negative, because the viscous stress resists the vortical motion. The only acceleration of M_z is brought by the pressure on the sidewalls normal to the y axis N_{py}, though the pressure on the sidewalls normal to the x axis N_{px} works against the vortical motion. Therefore, once the vortical motion arises, the vortical motion is accelerated autonomously by self-excitation cycles through the pressure on the sidewalls normal to the y axis.

Next, we examine how the induction of the vortex is achieved by the pressure on the sidewalls. It is the most comprehensive to observe the torque density on the sidewalls at $y = \pm 3/2$, which are caused by the pressure perturbation $\widetilde{p}$ obtained as the eigenfunction in the linear stability analysis. We denote the pressure as $p = \overline{p} + A\widetilde{p}$ with the disturbance amplitude A and $\widetilde{p}$. Then, we obtain $N_{py} = -2A\iint_{S_{y+}} x\widetilde{p}(x,3/2,z)dxdz$, where the symmetries $p(x,3/2,z) = p(-x,-3/2,z)$ and $\overline{p}(x,3/2,z) = \overline{p}(-x,3/2,z)$ are used. Thus, the torque N_{py} is determined solely by $\widetilde{p}$. The pressure perturbation along midheight of the sidewalls $\widetilde{p}(x,\pm 3/2,1/2)$ are shown in Figs. 6(a) and 6(c), respectively. We observe that the pressure perturbation $\widetilde{p}$ is an antisymmetric function of x and that it drives the fluid to rotate counterclockwise. We further confirm the driving mechanism by drawing the torque density per unit area $\widetilde{n}_{py}(x,\pm 3/2,1/2)$ $[= \mp x\widetilde{p}(x,\pm 3/2,1/2)]$ along midlines $(z = 1/2)$ shown in Figs. 6(a) and 6(c) (dotted line). It is evident that the torque density is positive over both sidewalls. This is also confirmed from Fig. 6(b), where contours of the torque density $\widetilde{n}_{py}(x,\pm 3/2,z)$ are shown. The torque density $\widetilde{n}_{py}(x,\pm 3/2,z)$ is a symmetric function of x and positive everywhere. We found the torque N_{py} has the same sign as the angular momentum of the disturbance and its strength $|N_{py}|$ is proportional to the magnitude A of the disturbance itself. This indicates self-excitation of the vortical motion. This self-excitation is the key mechanism of the generation and maintenance of the bathtub vortex. This pressure distribution leading to self-excitation is caused by the two small vortices adjacent to the sidewalls observed in Fig. 4.

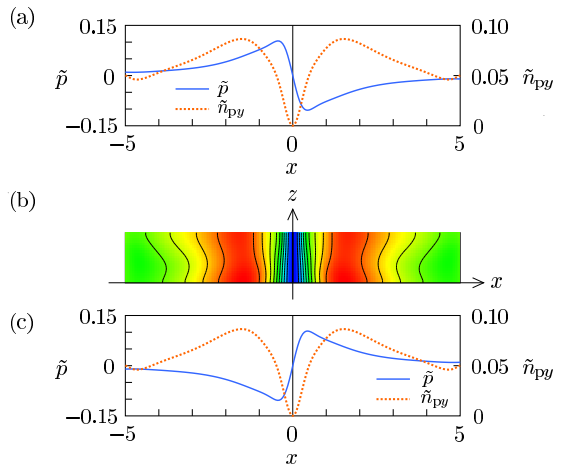

FIG. 6. (Color online) Pressure perturbation and torque density on the sidewalls. Re = 65; Ro = ∞. (a), (c) Pressure (solid line) and torque density (dotted line) along the center line at midheight of the sidewalls. (b) Torque density on the sidewalls (the same on $\pm 3/2$). (a) $y = 3/2$, (c) $y = -3/2$.

[1] A. H. Shapiro, Nature (London) **196**, 1080 (1962).
[2] L. M. Trefethen, R. W. Bilger, P. T. Fink, R. E. Luxton, and R. I. Tanner, Nature (London) **207**, 1084 (1965).
[3] N. Yokoyama, Y. Maruyama, and J. Mizushima, J. Phys. Soc. Jpn. **81**, 074401 (2012).
[4] T. Kawakubo, Y. Tsuchiya, M. Sugaya, and K. Matsumura, Phys. Lett. A **68**, 65 (1978).
[5] S. Shingubara and T. Kawakubo, J. Phys. Soc. Jpn. **53**, 1026 (1984).
[6] S. Shingubara, K. Hagiwara, R. Fukushima, and T. Kawakubo, Fluid Dyn. Res. **3**, 219 (1988).
[7] A. Andersen, T. Bohr, B. Stenum, J. J. Rasmussen, and B. Lautrup, Phys. Rev. Lett. **91**, 104502 (2003).
[8] See Supplemental Material at http://link.aps.org/supplemental/10.1103/PhysRevE.90.041002 for an assessment of the numerical accuracy of our numerical code.